DE GRUYTER OPEN

Chemically synthesized PbS nanoparticulate thin films for a rapid NO$_2$ gas sensor

VISHAL V. BURUNGALE[1], RUPESH S. DEVAN[2], SACHIN A. PAWAR[3], NAMDEV S. HARALE[1],
VITHOBA L. PATIL[1], V. K. RAO[4], YUAN-RON MA[2], JO EUN AE[3], JIN H. KIM[3],
PRAMOD S. PATIL[1*]

[1]Thin Film Materials Laboratory, Department of Physics, Shivaji University Kolhapur-416004, M.S., India

[2]Department of Physics, National Dong Hwa University, Hualien-97401, Taiwan, ROC

[3]Department of Materials Science and Engineering, Chonnam National University, Gwangju-500757, South Korea

[4]Defence Research & Development Establishment, Jhansi Road, Gwalior 474 002, India

Rapid NO$_2$ gas sensor has been developed based on PbS nanoparticulate thin films synthesized by Successive Ionic Layer Adsorption and Reaction (SILAR) method at different precursor concentrations. The structural and morphological properties were investigated by means of X-ray diffraction and field emission scanning electron microscope. NO$_2$ gas sensing properties of PbS thin films deposited at different concentrations were tested. PbS film with 0.25 M precursor concentration showed the highest sensitivity. In order to optimize the operating temperature, the sensitivity of the sensor to 50 ppm NO$_2$ gas was measured at different operating temperatures, from 50 to 200 °C. The gas sensitivity increased with an increase in operating temperature and achieved the maximum value at 150 °C, followed by a decrease in sensitivity with further increase of the operating temperature. The sensitivity was about 35 % for 50 ppm NO$_2$ at 150 °C with rapid response time of 6 s. T90 and T10 recovery time was 97 s at this gas concentration.

Keywords: *NO$_2$ sensor; PbS; XRD; SILAR*

1. Introduction

NO$_2$ is a reddish brown gas with a pungent and irritating odor. All types of combustion in air produce oxides of nitrogen among which NO$_2$ is the main component. NO$_2$ when transforms in the air forming nitric acid causes lake acidification, metal corrosion, fabrics fading and rubber degradation. It can also damage trees, crops; therefore, the production of nitric acid in air can cause substantial losses. Not only nitric acid but also NO$_2$ in air serves as one of the precursors for nitrates, which contribute to increased respirable particle level in the atmosphere [1]. So, taking into consideration all mentioned facts, the development of a stable NO$_2$ gas sensor that could detect low concentrations of NO$_2$ with high sensitivity is highly desirable. Such NO$_2$ gas sensors can be used for environmental monitoring and early warning systems. In general, different materials and thin films used for detection of NO$_2$ gas in ambient air are based on metal oxides [2–12], porous silicon [13], SiC [14] and carbon nanotubes [15–17]. These traditional chemiresistive sensors based on semiconducting oxides have good sensitivity but they work efficiently only in the temperature range of 200 to 650 °C [18–20]. This high operating temperature enhances both power consumption and safety issues. All limitations stated above motivated researcher community to develop rapid, sensitive gas sensor which will work at moderate operating temperatures.

There are very few research articles which are dedicated to pristine PbS as NO$_2$ gas sensor. Nevertheless, some research groups such as Kaci et al. utilized nanostructured PbS thin film deposited by chemical bath deposition method as a sensing element for detection of NO$_2$ gas at room temperature. In that work different additives, such as

---
*E-mail: patilps_2000@yahoo.com

organic substances were introduced into the reaction bath in order to improve sensitivity of the sensing device [21]. Recently Liu et al. reported physically flexible and fast response gas sensor based on colloidal PbS quantum dots, having response time of 4 s [22]. This device consisted of a paper on which PbS quantum dots were spin coated and it worked at room temperature. But synthesis of quantum dots is a very tedious process and mechanical stability of the paper based sensors in harsh conditions is dubious. So, the development of a robust gas sensor having rapid response is indispensable. In this work we have deposited PbS thin film on glass substrate by cost efficient and simple SILAR method which can be used as a robust PbS based gas sensor. The NO_2 gas sensors based on these PbS thin films have rapid response time of 6 s at moderate operating temperature.

2.   Experimental

At first, 10 mL of 30 % ammonia solution with 40 mL of 0.25 M lead acetate [$Pb(CH_3COO)_2 \cdot 3H_2O$], (Beaker I) and 50 mL of 0.25 M thiourea [$(NH_2)_2CS$], (Beaker III) solution were taken in two different beakers which were kept in a constant temperature (i.e. ∼60 °C) bath for 15 minutes. In another beaker (Beaker II) double distilled water was taken and this beaker was kept in the ultrasonic bath. A set of five glass substrates separated by spacers was immersed in the beaker containing 10 mL of 30 % ammonia solution with 0.25 M lead acetate [$Pb(CH_3COO)_2 \cdot 3H_2O$] for 55 s, which was further inserted for ultrasonic treatment in the beaker containing double distilled water (Beaker II) for 5 s. After this treatment, the set of five substrates was immersed in the thiourea solution and then it was subjected to ultrasonic treatment in the beaker containing double distilled water for 5 s (Beaker IV). In this way, one deposition cycle of 2 minutes was completed. Schematic illustration of the SILAR method is given in Fig. 1. The mentioned procedure was repeated for several times. To get samples of five different thicknesses, the substrates were taken out after a specific number of cycles. Finally, the thin films were rinsed with double
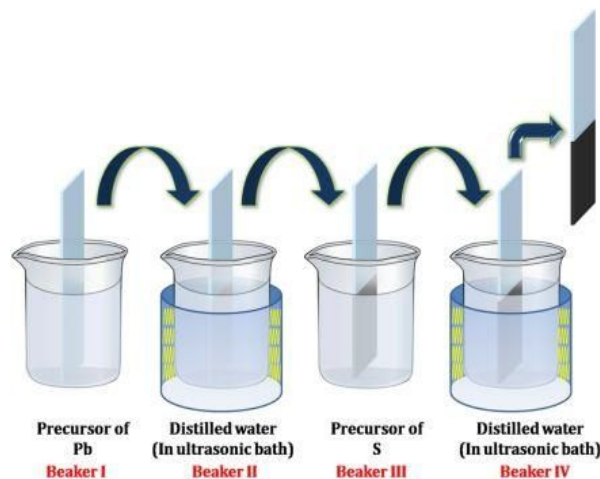
Fig. 1. A schematic showing a typical SILAR technique for deposition of PbS on glass substrate from chemical solutions containing cationic and anionic precursors.

distilled water and allowed to dry at room temperature to get well adherent and good quality PbS thin films with different thicknesses. PbS thin films deposited at 0.10, 0.15, 0.20, 0.25 and 0.30 M precursor concentrations are denoted as $PbS_{0.10}$, $PbS_{0.15}$, $PbS_{0.20}$, $PbS_{0.25}$ and $PbS_{0.30}$, respectively.

The X-ray diffraction (XRD) spectra of the films were recorded using X-ray diffractometer (Bruker AXS D2 PHASER model). The thickness of these films was measured using AMBIOS Make XP-1 model of surface profiler with 1Å vertical resolution. The elemental information about the films was analyzed using an X-ray photoemission spectroscopy Thermo K-Alpha XPS with multi-channel detector, which had high photonic energy, ranging from 0.1 to 3 keV. The surface morphology was examined using field emission scanning electron microscopy (FESEM JEOL JSM-6500F).

3.   Results and discussion

The X-ray diffraction patterns of the PbS thin films are shown in Fig. 2. The PbS samples are polycrystalline in nature and exhibit FCC structure. The well-defined peaks along (1 1 1), (2 0 0), (2 2 0), (3 1 1), (2 2 2), (3 3 1), (4 2 0), and (4 2 2) reflections are observed in the XRD patterns. The
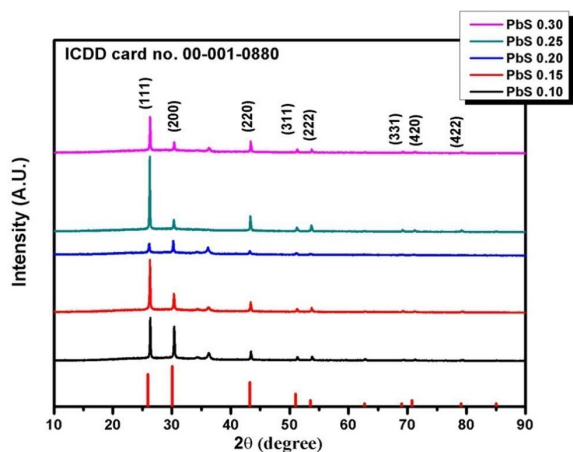
Fig. 2. X-ray diffraction patterns of PbS thin films deposited at different precursor concentrations.
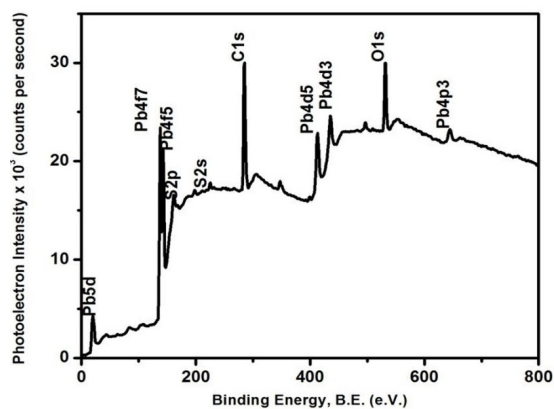
Fig. 3. Full scan XPS spectra of PbS$_{0.25}$ thin film.
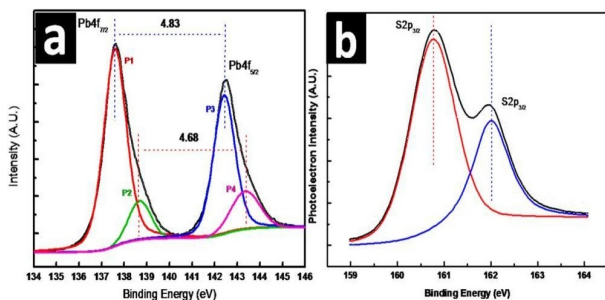
Fig. 4. High resolution XPS spectra of (a) Pb(4f) and (b) S(2p) core levels of the PbS$_{0.25}$ thin film. The XPS spectra are decomposed via Voigt curve fitting.

vigorous and sharp peaks are observed in the XRD patterns of all PbS samples, which suggests that the

samples are well crystallized [23]. It can be inferred from Fig. 2 that the preferred orientation growth of all PbS thin films deposited at different precursor concentrations is along the <1 1 1> direction. The absence of any other prominent diffraction peaks suggests that no other crystalline phases, such as oxides, hydroxides or carbonates of Pb, exist with detectable concentration within the deposited PbS layers.

Quantitative analysis of electronic structures and chemical states of the PbS films was performed by XPS. The values of the binding energy were calibrated utilizing C 1s peak (284.8 eV) as the internal standard. Fig. 3 shows a full scan XPS spectrum of PbS$_{0.25}$. The spectrum shows the presence of Pb and S as expected. In addition to Pb and S there are also peaks of C and O. The extra peaks are mainly due to exposure of the films to the air after synthesis. The molecules adsorbed from the atmosphere, such as water and carbon dioxide contributed to the C and O peak intensities. Fig. 4 illustrates the Pb(4f) and S(2p) XPS spectra for the PbS$_{0.25}$ thin film. The double peaks of the Pb(4f) and S(2p) in the XPS spectrum shown in Fig. 4a and Fig. 4b, respectively, suggest that the PbS thin film is mainly composed of PbS stoichiometric compound. To precisely determine the features of the double peaks of the Pb(4f$_{7/2}$) and Pb(4f$_{5/2}$), the XPS spectrum was decomposed via Voigt curve fitting following Shirley background subtraction. The results indicate a perfect fit to the four peaks (i.e. P1, P2, P3 and P4), where P1 and P3 correspond to the Pb (4f$_{7/2}$) and Pb (4f$_{5/2}$) core levels of the Pb^{2+} cations associated with PbS formation. They are located at the binding energies of 137.59 and 142.42 eV, respectively. Furthermore, P2 and P4 correspond to the core levels of the Pb^{2+} cation associated with PbO formation. The energy separation between the peak P1 and P3 is 4.83 eV while that of P2 and P4 is 4.68 eV. The energy separation of 4.83 eV reflects a vigorous binding between the Pb and S atoms. Moreover, the peaks P1 and P3 have much larger intensity than that of P2 and P4. This again suggests that the thin films are mainly composed of PbS compound. The S(2p) XPS spectrum of PbS thin film is shown in Fig. 4b.
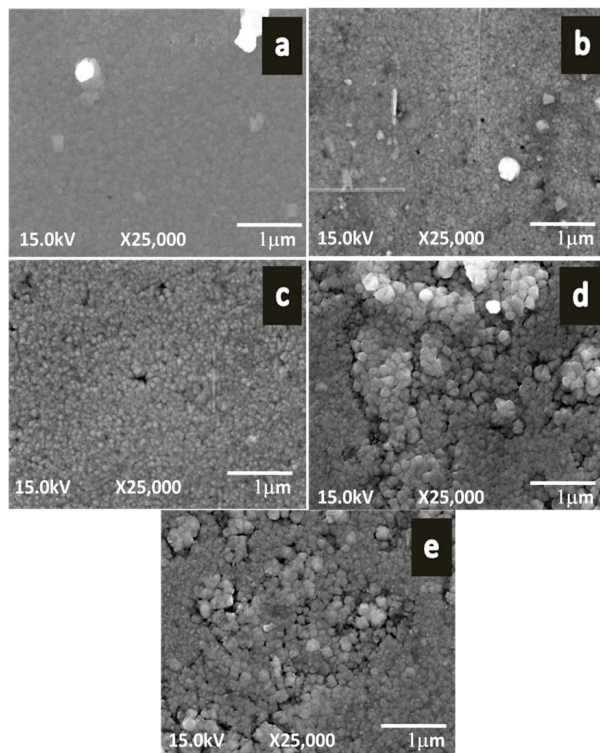
Fig. 5. FE-SEM micrographs of (a) $PbS_{0.25}$ (b) $PbS_{0.25}$ (c) $PbS_{0.25}$ (d) $PbS_{0.25}$ and (e) $PbS_{0.25}$ films at 25,000 magnification.

Fig. 6. A schematic showing typical plane and rough surface.
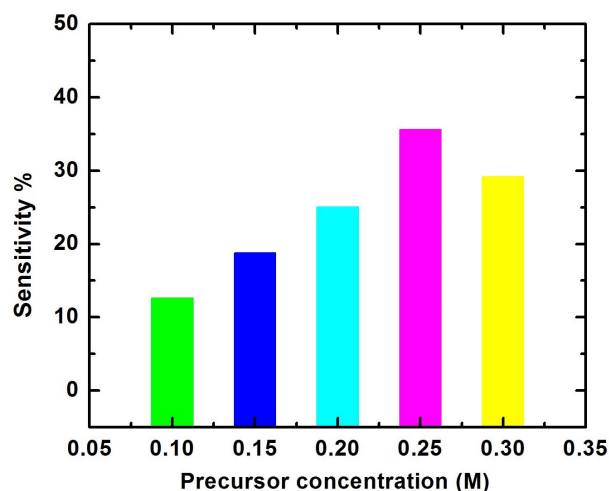
Fig. 7. Variation of sensitivity with precursor concentration in PbS thin films at 150 °C.

The double peak in the S(2p) XPS spectrum again confirms that the thin film is composed of pristine stoichiometric PbS compound without formation of S-oxide. The double peak featured S(2p) spectrum was decomposed via Voigt curve fitting following Shirley background subtraction. The results show a fit to two peaks located at 160.76 eV and 162 eV, respectively that correspond to the $S(2p_{3/2})$ and $S(2p_{1/2})$ core levels of the S^{2+} cations associated with PbS formation. Generally, the XPS spectra attest that the thin film is mainly composed of PbS, with minor traces of PbO compound.

Fig. 5 shows typical FESEM images of $PbS_{0.10}$, $PbS_{0.15}$, $PbS_{0.20}$, $PbS_{0.25}$ and $PbS_{0.30}$ thin films. In Fig. 5d compact grains of $PbS_{0.25}$ thin film are clearly visible. The size of the nanoparticles is about 100 nm.

PbS thin films deposited at different concentrations of precursors of lead and sulfur have been exposed to NO_2 gas at 150 °C temperature for determining their gas sensing properties. Fig. 7 shows that $PbS_{0.25}$ film has the highest sensitivity. The $PbS_{0.25}$ film has the thickness of 232.9 nm. The FE-SEM images of the PbS sample reveal that $PbS_{0.25}$ has relatively rough surface in comparison to other films so it favors enhanced gas adsorption [24, 25]. A schematic exhibiting the comparison between a plane and rough surface is given in Fig. 6. As can be observed in Fig. 6, due to the roughness, the net surface area of the film gets increased which will result in the increased number of sites for adsorption of gas molecules on the surface of the film.
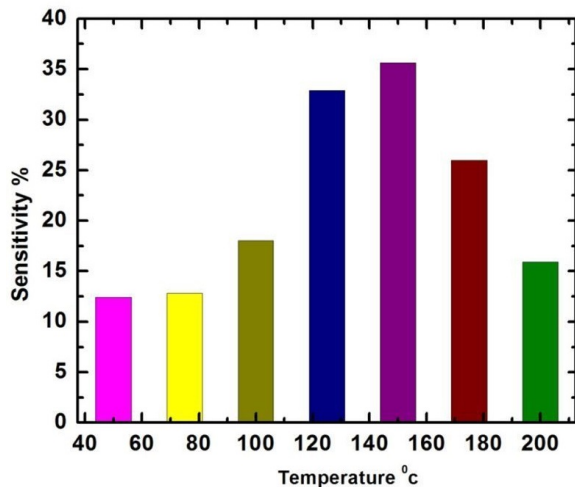
Fig. 8. Variation of NO$_2$ gas response with operating temperature at relative humidity of 60 to 65 %.
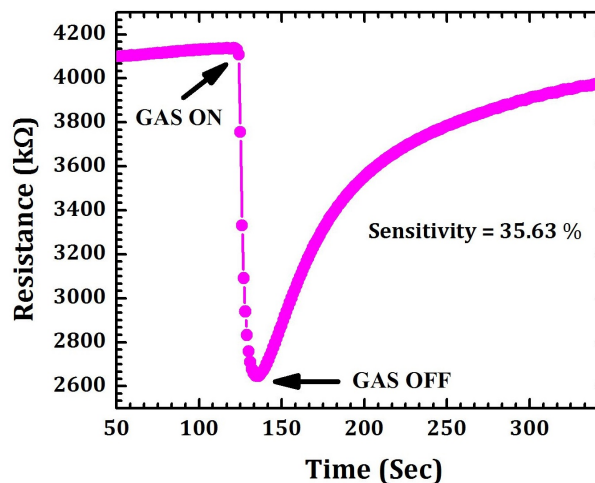
Fig. 10. Time response characteristics of a sensor of PbS$_{0.25}$ film to NO$_2$ at concentration 50 ppm.
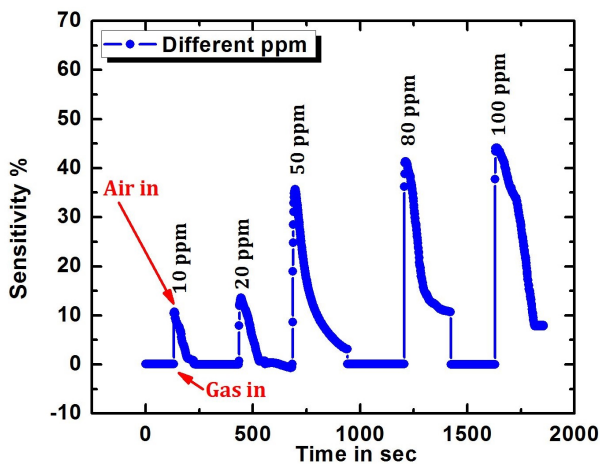
Fig. 9. Variation of NO$_2$ gas response with NO$_2$ gas concentration at relative humidity of 60 to 65 %.

The sensing properties of the sensor based on the as-prepared PbS sample were also examined in terms of sensitivity with the reference to operating temperature and NO$_2$ gas concentration. The response of the sensor, S, is defined as S $=$ (R$_{gas}$ $-$ R$_{air}$)/R$_{gas}$ for R$_{gas}$ $>$ R$_{air}$ and S $=$ (R$_{air}$ $-$ R$_{gas}$)/R$_{air}$ for R$_{air}$ $>$ R$_{gas}$, where R$_{gas}$ and R$_{air}$ are the resistances of the sensor exposed to the gas-air mixture and air alone, respectively. In present study R$_{air}$ $>$ R$_{gas}$ hence, sensitivity is calculated by the formula S $=$ (R$_{air}$ $-$ R$_{gas}$)/R$_{air}$. In order to optimize the operating temperature, the gas

sensitivity of the sensor to 50 ppm NO$_2$ gas was measured at different operating temperatures, from 50 to 200 °C, and the results are shown in Fig. 8. The gas sensitivity increased with an increase in operating temperature and achieved a maximum value of 35 % at 150 °C and at relative humidity of about 60 to 65 %. With further increase of the operating temperature a decrease in sensitivity was observed. To examine further the sensing characteristics of the sensor, the optimal operating temperature of 150 °C was chosen for NO$_2$ sensing. The effect of NO$_2$ gas concentration on the sensitivity of the PbS thin film has also been tested. In Fig. 9 it is observed that for 10, 20, 50, 80 and 100 ppm concentration of NO$_2$, the sensitivity of the PbS film is 10.62, 13.60, 35.63, 41.31 and 44.09, respectively, and the response time of the PbS film for 10, 20, 50, 80 and 100 ppm concentration of NO$_2$ is 12, 16, 6, 6, 2s, respectively. So, it is observed that as the concentration of NO$_2$ gas increases the sensitivity also increases and the response time decreases. This is quite obvious since with increasing concentration the adsorption of gas molecules increases which finally results in enhanced sensitivity. When the temperature increased from 50 to 200 °C, the increase in the gas sensitivity could be roughly explained by the increase in the surface reaction rate (NO$_{2(gas)}$ + e$^-$ $\rightarrow$ NO$_{2(ads)}^-$). When the

temperature was further increased, the response might be limited by the low diffusion depth and began to decrease [26, 27]. At the optimized operating temperature (150 °C), the optimum balance between the adsorption reaction and diffusion depth for the NO₂ gas molecules was studied. As depicted in Fig. 10 the response time of optimized sample was 6 s. making this device one of the most rapid NO₂ gas sensor ever reported [28]. The repeatability of the sensing performance has also been tested. Fig. 11 shows the time response characteristics for five consecutive cycles of the sensor made of PbS$_{0.25}$ film to NO₂ at a concentration of 50 ppm. It is observed that the sensitivity of 35 % and response time of 6 s remain almost constant for all five cycles.
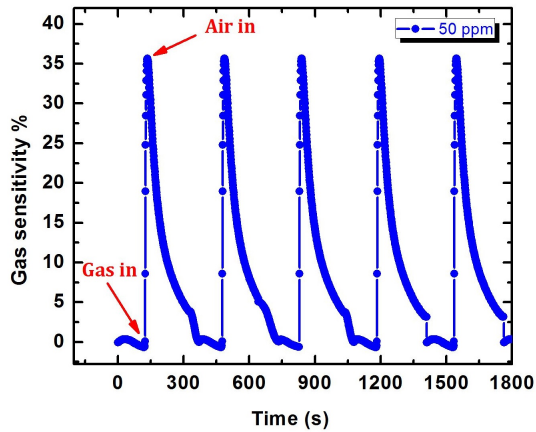
Fig. 11. Time response characteristics for five consecutive cycles of a sensor of PbS$_{0.25}$ film to NO₂ at a concentration of 50 ppm.

Gas sensing mechanism of semiconductor gas sensors is based on the conductivity change of the sensing materials. The oxygen molecules play consequential role in the sensing mechanism. The oxygen molecules adsorb on the surface and capture the electrons from the conduction band of the semiconductor which leads to its ionosorption in molecular (O_2^-) and atomic (O^-, O^{2-}) forms [29]. The adsorption kinematics are explained as follows [30]:

$$O_{2(gas)} \leftrightarrow O_{2(adsorbed)} \qquad (1)$$
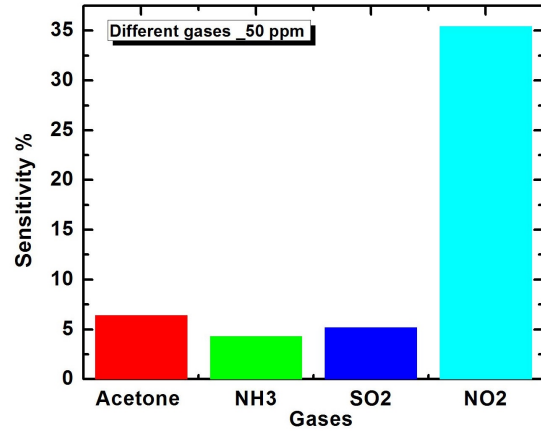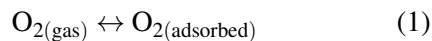
Fig. 12. Variation of sensitivity of PbS thin film to acetone, NH₃, SO₂ and NO₂ at gas concentration of 50 ppm at 150°C.

$$O_{2(adsorbed)} + e^- \leftrightarrow O_2^-, \qquad (2)$$

$$O_2^- + e^- \leftrightarrow 2O^- \qquad (3)$$

$$O^- + e^- \leftrightarrow O^{2-} \qquad (4)$$
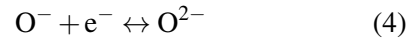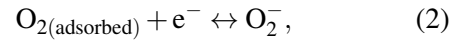
When atmospheric oxygen molecules chemisorb on the surface of material by trapping electrons, depletion region is formed. When sensor is exposed to strong oxidizing NO₂ gas, it reacts with ionosorbed oxygen ions leading to the formation of adsorbed NO_2^- (ads) [31] as follows:

$$NO_{2(gas)} + e^- \rightarrow NO_{2(ads)}^- \qquad (5)$$

$$NO_{2(gas)} + O_{2(ads)}^- + 2e^- \rightarrow NO_{2(ads)}^- + 2O_{(ads)}^- \qquad (6)$$
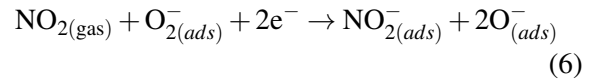
The reaction with the chemisorbed oxygen and also independent trapping of electrons from conduction band of the semiconductor by strong oxidizer NO₂, give rise to an increase in the hole concentration. As PbS is a p-type semiconductor, the increment in hole concentration results in an increased electrical conductance of PbS material. The cross sensitivity of PbS sample has been tested for different gases i.e. acetone, NH₃ and SO₂. Fig. 12 shows the variation of sensitivity of PbS
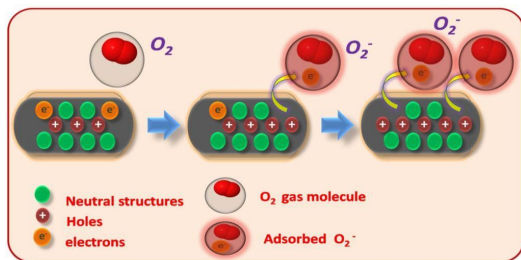
Fig. 13. Schematic illustration of adsorption of O_2 gas molecules on the grains of PbS material.
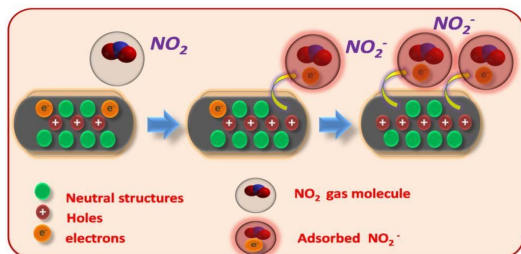
Fig. 14. Schematic illustration of adsorption of NO_2 gas molecules on the grains of PbS material.
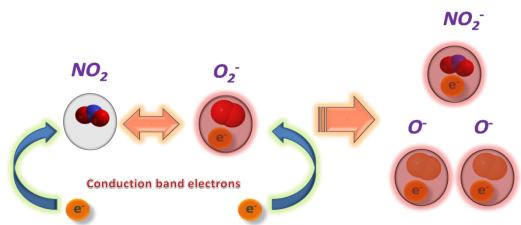
Fig. 15. Schematic illustration of removal of conduction band electrons by adsorption of O_2 and NO_2 gas molecules and subsequent reactions on the grains of PbS material.

sample for the mentioned gases. It is observed that maximum sensitivity at 50 ppm gas concentration is achieved for NO_2 gas. The schematic illustration of gas sensing mechanism is given in Fig. 13, Fig. 14 and Fig. 15. Fig. 13 shows adsorption of O_2 on the surface of PbS when it is exposed to ambient air atmosphere, while Fig. 14 illustrates the mechanism of adsorption of NO_2 molecule on the PbS surface; here simultaneous adsorption of O_2 is not shown. In Fig. 15 the possible reaction between adsorbed NO_2 and O_2^- is schematically presented.

4. Conclusions

PbS based NO_2 gas sensors with PbS thin films prepared at different precursor concentrations by a simple and cost efficient SILAR method has been reported. The response of the sensor was characterized at various temperatures and concentrations of NO_2 gas. Experimental results revealed that the $PbS_{0.25}$ sample shows the most efficient response to NO_2 gas. In addition, the PbS based sensors work the most efficiently at 150 °C. The fastest response time (T90) of 6 s has been observed for the same sample which makes this device one of the most rapid and effective NO_2 gas sensor ever reported.

References

[1] http://www.airqualityontario.com/science/pollutants/nitrogen.php.
[2] LLOBET E., MOLAS G., MOLINAS P., CALDERER J., VILANOVA X., BREZMES J., SUEIRAS J.E., CORREIG X., *J. Electrochem. Soc.*, 147 (2000), 776.
[3] SHISHIYANU S.T., SHISHIYANU T.S., LUPAN O.I., *Sens. Actuators B*, 113 (2006), 468.
[4] WANG X., MIURA N., YAMAZOE N., *Sens. Actuators B*, 66 (2000), 74.
[5] MAEKAWA T., TAMAKI J., MIURA N., YAMAZOE N., *Chem. Lett.*, 21 (1992), 639.
[6] XU C.N., MIURA N., ISHIDA Y., MATSUDA K., YAMAZOE N., *Sens. Actuators B*, 65 (2000), 163.
[7] PEDROSA J.M., DOOLING C.M., RICHARDSON T.H., HYDE R.K., HUNTER C.A., MARTIN M.T., CAMACHO L., *J. Mater. Chem.*, 9 (2002), 2659.
[8] WANG X., MIURA N., YAMAZOE N., *Sens. Actuators B*, 66 (2000), 74.
[9] MARQUIS B.T., VETELINO J.F., *Sens. Actuators B*, 77 (2001), 100.
[10] PENZA M., TAGLIENTE M.A., MIRENGHI L., GERARDO C., MARTUCCI C., CASSANO G., *Sens. Actuators B*, 50 (1998), 9.

[11] PENZA M., MARTUCCI C., CASSANO G., *Sens. Actuators B*, 50 (1998), 52.

[12] KIM T.S., KIM T.B., YOO K.S., SUNG G.S., JUNG H.J., *Sens. Actuators B*, 62 (2000), 102.

[13] BARATTO C., FAGLIA G., COMINI E., SBERVEGLIERI G., TARONI A., LA FERRARA V., QUERCIA L., DI FRANCIA G., *Sens. Actuators B*, 77 (2001), 62.

[14] CONNOLLY E.J., TIMMER B., PHAM H.T.M., GROENEWEG J., SARRO P.M., OLTHUIS W., FRENCH P.J., *Sens. Actuators B*, 109 (2005), 44.

[15] SUHIRO J., ZHOU G., HARA M., *J. Phys. D Appl. Phys.*, 36 (2003), 109.

[16] CHANG H., LEE J.D., LEE S.M., LEE Y.H., *Appl. Phys. Lett.*, 79 (2001), 3863.

[17] CHOPRA S., PHAM A., GAILARD J., PARKER A., RAO A.M., *Appl. Phys. Lett.*, 80 (2002), 4632.

[18] YAMAZOE N., *Sens. Actuators B*, 108 (2005), 2.

[19] CHEN X., JING X., WANG J., LIU J., SONG D., LIU L., *Superlattices Microstruct.*, 63 (2013), 204.

[20] LUPAN O.I., SHISHIYANU S.T., SHISHIYANU T.S., *Superlattices Microstruct.*, 42 (2007), 375.

[21] KACI S., KEFFOUS A., HAKOUMA S., TRARI M., MANSRI O., MENARI H., *Appl. Surf. Sci.*, 305 (2014), 740.

[22] LIU H., LI M., VOZNYY O., HU L., FU Q., ZHOU D., XIA Z., SARGENT E.H., TANG J., *Adv. Mater.*, 26 (17) (2014), 2718.

[23] CHENG T., FANG Z., ZOU G., HU Q., HU B., YANG X., ZHANG Y., *Bull. Mater. Sci.*, 29 (7) (2006), 701.

[24] KAMBLE A.S., PAWAR R.C., TARWAL N.L., MORE L.D., PATIL P.S., *Mater. Lett.*, 65 (2011), 1488.

[25] KAMBLE A.S., PAWAR R.C., PATIL J.Y., SURYAVANSHI S.S., PATIL P.S., *J. Alloy. Compd.*, 509 (2011), 1035.

[26] BAI S., ZHANG K., LUO R., LI D., CHEN A., LIU C.C., *J. Mater. Chem.*, 22 (2012), 12643.

[27] YOU L., SUN Y.F., MA J., GUAN Y., SUN J.M., DU Y., LU G.Y., *Sens. Actuators B*, 157 (2011), 401.

[28] AFZAL A., CIOFFI N., SABBATINI L., TORSI L., *Sens. Actuators B*, 171 (2012), 25.

[29] BELYSHEVA T.V., BOGOVTSEVA L.P., KAZACHKOV E.A., SEREBRYAKOVA N.V., *J. Anal. Chem.*, 58 (2003), 583.

[30] SAHAY P.P., TEWARI S., *J. Mater. Sci.*, 40 (2005), 4791.

[31] WETCHAKUN K., SAMERJAI T., TAMAEKONG N., LIEWHIRAN C., SIRIWONG C., KRUEFU V., WISITSORAAT A., TUANTRANONTB A., PHANICHPHANT S., *Sens. Actuators B*, 160 (2011), 580.